

A Spatial Frequency-Doubling Illusion-Based Pattern Electroretinogram for Glaucoma

Teddy Maddess,¹ Andrew Charles James,¹ Ivan Goldberg,² Stephen Wine,² and Jeffrey Dobinson²

PURPOSE. A pattern electroretinogram (PERG) in which stimuli displaying the frequency-doubling (FD) illusion are presented simultaneously to multiple parts of the visual field was evaluated for its ability to diagnose glaucoma. This multiregion FD PERG is referred to in the current study as the MFP.

METHODS. The nine stimulus regions were temporally modulated at incommensurate frequencies typically producing an FD percept. Two other spatial scales of the stimuli were also investigated. The sensitivity and specificity of MFP were examined using linear and quadratic discriminant methods.

RESULTS. Even with the simpler linear discriminant classification, sensitivities and specificities of 100% were obtained in eyes with moderate to severe glaucoma. Of eyes with glaucoma strongly suspected, 67% were classified as being glaucomatous. Stimulus patterns having differing spatial scales produced different PERG visual field dependencies.

CONCLUSIONS. The differing results for the 16-fold change in spatial scale may reflect the accessing of different mechanisms. The MFP method appears to have significant value for the diagnosis of glaucoma. (*Invest Ophthalmol Vis Sci.* 2000;41:3818-3826)

Transection of the optic nerve leads to degeneration of the inner retina and a declining pattern electroretinogram (PERG) in cats,¹ monkeys,² and humans.³ The PERG has components resulting from current flows in the vicinity of the inner plexiform (IPL) and ganglion cell layers.^{4,5} There are several types of retinal ganglion cells⁶ and many types of amacrine cells with processes in the IPL.⁷⁻¹⁰ The PERG is thus the sum of currents from a variety of sources within the proximal retina (for review see Reference 11). Which of these signals, if any, is related to glaucoma and why?

Long-term studies provide evidence that the PERG has predictive value in glaucoma,¹²⁻¹⁴ but what might be the best stimulus arrangement for glaucoma diagnosis? Trick¹⁵ showed that increasing the temporal frequency of contrast modulation from 1 to 8 Hz improved discrimination of normal subjects and patients with primary open-angle glaucoma (POAG) when using check sizes that have fundamental spatial frequencies in the range 0.18 to 1.41 cyc/deg (see also Reference 16). Marx et al.¹⁷ found that decreasing spatial frequency from 3.5 to 0.5 cyc/deg improved sensitivity in experimental glaucoma for stimulation at 6 Hz. Johnson et al.¹⁸ showed that spatial frequencies of approximately 0.18 cyc/deg (i.e., 2° checks) modulated at 10 Hz discriminated glaucomatous primate eyes well.

The reader is further referred to an excellent review on the use of evoked potentials in assessing glaucoma.¹⁹

These studies share one factor: The visual stimulus is presented at the same scale to all parts of the retina, thus ignoring the 50-fold decline in ganglion cell density between 2° and 10° eccentricity.^{20,21} There is increasing evidence that there is diffuse as well as local ganglion cell loss in glaucoma.²²⁻²⁵ Anatomical²⁵ and PERG studies^{12,13,26} indicate macular as well as peripheral retinal damage in early glaucoma, and the potential for central retinal involvement therefore should not be ignored. At the same time, peripheral scotomas are a diagnostic feature of glaucoma.²⁷ Ideally, several image regions should be tested, and the size of these regions and the scale of any textures contained in them should be tailored to retinal ganglion cell density and characterization of both diffuse and sectoral losses. Some attempts have been made in this area, such as use of appropriately scaled dot patterns²⁸ or separate recordings for different check sizes.^{26,29} In multifocal visual evoked potential (VEP) studies of glaucoma,³⁰ the check sizes used were M-scaled.

The issue of spatial scale is separate from whether there is a component of the PERG that is suited to glaucoma diagnosis. There is considerable evidence, both from experimental glaucoma^{25,31} and human POAG,³²⁻³⁵ that large retinal ganglion cells are disproportionately damaged. In primates the parasol cells³⁶ project to the magnocellular layers of the dorsal lateral geniculate nucleus (dLGN)^{6,37} and so are frequently referred to as M cells. The M pathway contains (at least) two functional classes that are similar to cat X and Y cells.^{6,39} Between 5% and 20% of dLGN M cells respond with a nonlinear Y-type response³⁹⁻⁴² thus, the term M_y cells. The responses of LGN units largely reflect the characteristics of their retinal ganglion cell inputs.⁴³⁻⁴⁷ Subpopulations of parasol cells that are either

From the ¹Centre for Visual Sciences, Research School of Biological Sciences, Australian National University, Canberra; and the ²Prince of Wales Hospital, Sydney, Australia.

Submitted for publication June 10, 1999; revised January 26 and June 19, 2000; accepted July 11, 2000.

Commercial relationships policy: P (TM, ACJ); N (all others).

Corresponding author: Teddy Maddess, Centre for Visual Sciences, Research School of Biological Sciences, Australian National University, Canberra ACT 0200, Australia. ted.maddess@anu.edu.au

coupled or not coupled to amacrine cells,⁴⁸ a feature that discriminates cat X and Y cells,⁴⁹ may have some relation to the primate X and Y types. At least three studies indicate that M_y -cell receptive fields^{39,50} and axons^{39,40} (based on conduction velocities) are larger than those of M_x cells. Therefore, it seems that M_y cells may be larger than M_x cells.

From the perspective of glaucoma diagnosis it is perhaps more important that M_y cells appear to have a very low retinal coverage factor,⁵¹⁻⁵³ so that loss of a single cell perhaps leads to a complete local loss of visual sensitivity at a given retinal location. These findings, in conjunction with some selective loss of larger ganglion cells in glaucoma, suggest that the M_y -cell subsystem should be accessed to monitor glaucoma.

How then should the M_y -cell class be accessed? One possibility is that the spatial frequency-doubling (FD) illusion⁵⁴⁻⁵⁶ may be related to M_y -cell function.^{52,53,57,58} The FD illusion is seen when subjects view spatially coarse sinusoidal gratings with a contrast that is modulated at 15 to 30 Hz⁵⁴⁻⁵⁶ or that are presented briefly.^{59,60} The nonlinearity describing the characteristic response component of Y cells has the same rectifying form as that governing the FD illusion (cf. References 61 and 54). Some investigators^{57,58,62} have shown that when FD is seen, the PERG signal becomes dominated by components with phase shifts characteristic of the retinal gain control signal operating on the nonlinear response component of Y cells.⁶³ This retinal gain control mechanism greatly increases the nonlinear responses of Y cells to stimuli combining low spatial frequencies and high temporal frequencies^{61,63-66,67} The nonlinear response component of Y cells is more amplified by retinal gain control than either the Y cells' own linear response or that of X cells,^{61,64,68,69} which might explain the appearance of the illusion. Also, we⁵³ have shown that the spatial density of the units subserving the FD illusion is very similar to the anatomic expectation for M_y cells. The ability of subjects with glaucoma to see the FD illusion is severely reduced.^{52,70-80} Evidence has been provided that FD stimuli are superior to wide-field flicker in detecting glaucoma.⁸¹ So, as might be predicted if the FD illusion corresponded to M_y -cell function, it appears that the strength of the FD illusion is highly correlated with glaucomatous damage.

Taking all the evidence into account, we created a visual stimulus that was correctly scaled with respect to M_y -cell density,⁵³ that exploited the FD illusion, and that had multiple, relatively large stimulus zones.⁷⁰ In a companion study⁸² we compared the MFP results with results from Humphrey Field Analyser (Humphrey, San Leandro, CA) examinations and a contrast threshold method using FD stimuli.⁷³

METHODS

Visual Stimuli and Data Analysis

Visual stimuli were presented on a model CCID 7551 monitor (Barco, Kortrijk, Belgium; mean luminance 45 candelas [cd]/m²). The monitor was calibrated weekly. Gamma correction was confirmed by nonlinear systems identification methods.⁶² Subjects viewed the monitor at 30 cm providing the stimulus layout illustrated in Figure 1. A green fixation spot was presented at the screen's center. The screen of the monitor was divided into nine zones or regions (Fig. 1; Fig. 3, inset). Each region contained an achromatic (6500° K) sinusoidal grating at 95% contrast. In most of the experiments, the grating orienta-

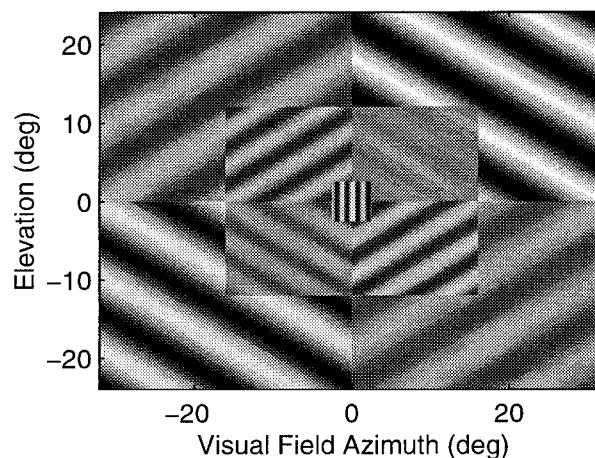


FIGURE 1. Illustration of the MFP stimulus. The spatial scale of the stimulus present on the monitor screen is demonstrated along with the scale of the gratings. The displayed spatial frequencies represent the input spatial frequencies, not the illusory second harmonic observed. For the so-called coarse and fine stimuli (Fig. 4), the spatial frequencies of all regions were scaled up or down by 4, whereas the region size remained fixed. The gratings are presented here at different contrasts to permit the 9 regions to be distinguished but could represent a single frame of the stimulus sequence, because contrast of the gratings was modulated asynchronously.

tion in regions 2 through 9 was such that the stripes of the gratings were normal to lines drawn from the center of the monitor to the four corners. The grating in central region 1 had vertical stripes. The scale of the gratings increased with eccentricity according to cell density.⁵³ Normally, gratings in the nine regions had the spatial frequencies: region 1, $\frac{3}{4}$ cyc/deg; regions 2 through 5, $\frac{1}{4}$ cyc/deg; and regions 6 through 9, $\frac{1}{8}$ cyc/deg. In some experiments the spatial frequency of all zones was scaled up or down by a factor of 4 to make so called coarse and fine stimulus patterns. The stimulus display was controlled by a program running on a Vista graphics board (Truevision, Shadeland Station, IN). Software for data acquisition, online analysis and data display was written in a commercially available program (Matlab; The MathWorks, Natick, MA).

Data Acquisition and Processing

To permit extraction of responses to the different regions while recording with one electrode, the contrast of each stimulus region was sinusoidally modulated in time, each region at a slightly different temporal frequency (described later). The MFP signals were amplified 125,000 times and sampled in synchrony with the video frames displayed on the monitor. Electrodes (ERG-Jet; Universo SA, La Chaux-de-Fonds, Switzerland) were used for the eye contact, and AgCl button electrodes were used for the indifferent and earth electrodes. The indifferent electrode was placed on the temple, and the ground on the cheekbone half way between the midline of the eye and the temple. Control experiments revealed no contamination by cortical potentials. The time base for the analogue-to-digital converter (ADC) sampling (Labmaster MDA, Scientific Solutions, Solon, OH; 16 bit) was the horizontal line-scan clock (45,473 Hz) supplied by the graphics board. The video frame rate was 101.50 Hz (noninterlaced), and there were 448 cycles of the horizontal line-scan clock per frame. A single stimulus

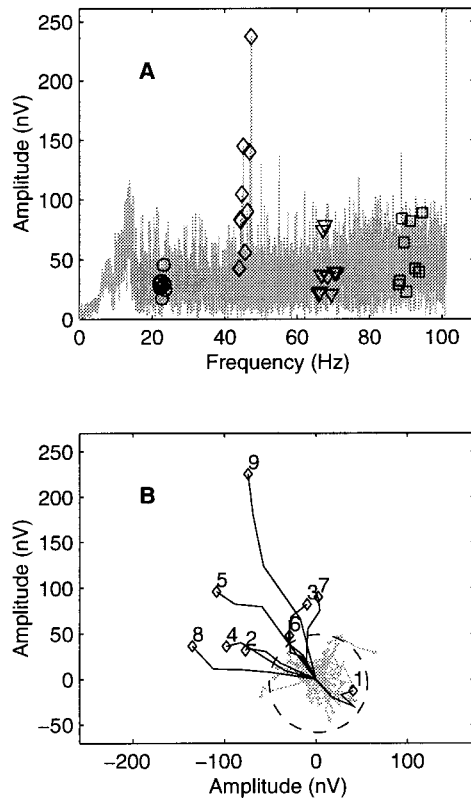


FIGURE 2. A sample MFP data set mimicking the display seen by the test operator. **(A)** An amplitude spectrum: (○) nine fundamentals, (◇) second, (▽) third, and (□) fourth harmonics. There is a component from the frame rate (101.50 Hz; *right*). **(B)** An Argand diagram showing the nine second harmonics in the complex plane (*numbered vector trajectories*). The four segments of each trajectory represent the gain and phase for each of the four trial responses, with gain scaled by $[1/4]$, so that that each trajectory is the vector mean, and its distance from the origin denotes the mean response amplitude. Regional interaction frequencies $f_i + f_j$ and noise frequencies (*gray lines terminated with small dots*) have random phase and therefore form random walks around the origin. The *dashed circle* is the 95% confidence limit computed from the noise frequencies. Thus, vectors escaping from the *dashed circle* with increasing trial number are significantly different from noise.

sequence contained 4096 frames of video providing an overall stimulus duration of 40.4 seconds. Response components were extracted by the fast Fourier transform (FFT), the run length providing a temporal frequency resolution Δf of 0.0248 Hz.

For the FFT signal extraction process to work, an orthogonal design was needed. That is to say, it was necessary for all nine stimulus frequencies (f_1, f_2 , and f_9) to contain an integral number of cycles over the 4096 video frames. Because we were interested in the second harmonics, it was also necessary that no two summed frequencies ($f_i + f_j$) should equal any of the nine second harmonic frequencies. If summed frequencies $f_i + f_j$ appeared in the record, they would represent interaction or light scattering between the stimulus zones, and these frequencies were therefore also monitored. The actual stimulus frequencies were the multiples: $\Delta f \cdot (889, 898, 904, 911, 921, 935, 947, \text{ and } 955)$. The resultant second harmonic signals thus ranged from 44.06 to 47.33 Hz (contrast reversals/sec).

We recorded several repeats of the 40.4-second stimulus sequence. An FFT of each record was computed, and the

resultant complex Fourier transfer coefficients were averaged. Figure 2 demonstrates graphically the output of the data acquisition program and the initial analysis. Figure 2A shows the amplitude spectrum highlighting the fundamental, second, third, and fourth harmonics. Figure 2B shows the second harmonics, numbered 1 through 9 and some other frequencies in the complex plane in an Argand diagram. For this part of the analysis, we extracted the second harmonics ($f_i + f_j = 2f_i$), the regional interaction frequencies ($f_i + f_j, i \neq j$), and all the remaining noise frequencies in the band f_1 to f_9 . In the Argand diagram, frequencies are represented as vectors for which the length from the origin represents signal amplitude and the orientation represents phase lag. Note in this case that because the stimulus frequencies were bunched (range, 1.8 Hz) differences in phase corresponded closely to differences in conduction delays. In the Argand representation if response vectors were concatenated from repeated runs and scaled by the number of repeats (i.e., take the vector average in the complex plane), then only responses with relatively constant phase would grow in amplitude. Noise frequencies would have random phase and so would stagger in a random walk around the origin. The coefficients from the noise frequencies thus form a bivariate normal distribution that can be used to measure the significance of the measured harmonics. In Figure 2B the noise frequency coefficients and regional interaction frequencies ($f_i + f_j, i \neq j$) lie inside the circle representing the 95% significance level. The derivation of that significance level is given in the next paragraph.

The actual significance of a frequency component is related to its amplitude, which is the modulus of the Fourier transform coefficient at that frequency, $A(f)$. A test of significance for a particular frequency can be performed as follows. Under a null hypothesis of no signal, the real and imaginary parts of the Fourier transform coefficients, $\text{Real}[A(f)]$ and $\text{Imag}[A(f)]$, are independent normal variates with zero mean and some variance σ^2 . The squared modulus of the coefficient $|A(f)|^2$ is then σ^2 times a χ^2 variate on 2 degrees of freedom. An estimate s^2 of σ^2 is obtained from frequencies not in the set of second-order stimulus frequencies, say with n degrees of freedom. An F-test is then performed on the quotient $(|A(f)|^2/2)/(s^2/n)$, with $(2, n)$ degrees of freedom. For large n the F-test is closely approximated by a χ^2 test, the test statistic being $|A(f)|^2/s^2$, with 2 degrees of freedom. This method was used to draw the circle denoting 95% confidence in Figure 2. Thus, a given frequency component is significant if, and only if, it lies outside the circle.

As can be seen (Fig. 2B), unlike the noise frequencies, the nine signal components had relatively constant phase and so over four runs had grown outside the significance level. In practice, the operator viewed the Argand diagram (Fig. 2B) and judged whether sufficient repeats had been obtained to ensure that most or all the signals from the nine regions exceeded the significance level. Preliminary experiments determined that all nine responses could be significant in as few as four repeats (as shown in Fig. 2B). Therefore, the operator was instructed to perform at least 4 repeats, but not more than 12, so that recording time did not exceed 10 minutes. The operator was instructed to stop after fewer than 12 repeats if all nine regional signals had reached 95% significance. These averaged responses were used for subsequent off-line analysis.

TABLE 1. Summary of Subject Data for the Four Diagnostic Groups

	Normal Subjects	Weakly Suspect	Strongly Suspect	Known Glaucoma
Number of eyes	12	36	15	14
Age (y)	59.25 ± 11.14	57.39 ± 10.37	60.47 ± 7.83	62.23 ± 10.09
VCDR contour	0.53 ± 0.18	0.58 ± 0.14	0.62 ± 0.20	0.80 ± 0.10
VCDR colour	0.46 ± 0.10	0.52 ± 0.17	0.55 ± 0.19	0.76 ± 0.13
Correction (D)	0.72 ± 0.18	0.61 ± 2.18	1.31 ± 1.68	0.99 ± 3.33
Correction (min:max)	-4.25:5.13	-5.00:5.25	-1.25:4.00	-7.00:5.75
Acuity (cf. 6)	5.90 ± 1.79	5.96 ± 1.94	6.50 ± 2.24	6.50 ± 2.23
MD (dl)	-3.53 ± 3.84	-1.44 ± 1.80	-1.41 ± 1.28	-6.64 ± 3.99
PSD (dl)	3.92 ± 3.18	2.19 ± 0.69	1.96 ± 0.60	6.18 ± 3.90
Pupil (mm)	3.25 ± 0.49	3.29 ± 0.51	3.11 ± 0.70	2.38 ± 0.74
Prior IOP (mm)	15.57 ± 1.51	25.56 ± 5.37	29.47 ± 7.68	32.80 ± 6.99
Test IOP (mm)	14.29 ± 2.50	20.00 ± 4.96	21.60 ± 3.46	19.38 ± 4.94

All errors are standard deviations. Vertical cup to disc ratios (VCDR) are given by contour and colour. Refraction is summarized on two rows, providing the means ± SD and the minimum:maximum. Corrected acuity is relative to 6/6, one subject with strongly suspected and one with glaucoma who were 6/18 were excluded to give a better impression of the typical acuity. The median for all groups was 6/6. The MD and PSD data are from HFA 24-2 perimetry (Humphrey, San Leandro, CA). The pupil data are diameters determined during the psychophysical tests.⁸² The prior IOP data are the highest recorded in the history of that subject in their history in millimeters of mercury. Test IOP was the pressure on the day.

Subjects

Right eyes of 77 subjects were tested. We used the 24-2 program of the Humphrey Field Analyzer (HFA; Humphrey, San Leandro, CA) to obtain standard perimetric visual field threshold data from the 77 subjects in the study group. By those and other previously described criteria⁷³ subjects were classified (initially by IG, and confirmed by SW and JD) into four groups: normal subjects, persons with glaucoma weakly suspected (weakly suspect group), persons with glaucoma strongly suspected (strongly suspect group), and persons with known glaucoma (glaucoma group). Of the glaucoma group, 12 of 14 met the strict HFA criteria of Caprioli⁸³ for glaucoma diagnosis; all met the moderate Caprioli criteria. Strongly suspect eyes did not meet either of these visual field criteria but had a highest ever recorded elevated intraocular pressure (IOP), determined by applanation tonometry, of more than 20 mm Hg and a glaucomatous change in the optic disc verified by repeated fundus camera photography of the optic disc over several years (by IG). For a more complete description of the clinical evaluation of these subjects see Maddess et al.⁷³

Six of the glaucoma group had a blockage-mechanism form of glaucoma, and the remainder had POAG. The group was part of a larger study on 330 subjects in which no effect of these differing glaucoma types was found for visual field thresholds obtained for FD stimuli.⁷³ Weakly suspect eyes had elevated IOP or suspect discs but had no observed change in the disc over several years. Disc condition was assessed by fundus photography, and vertical cup-to-disc ratios were evaluated by color and contour (see Table 1 of Reference 73). Further details of the diagnostic criteria are given elsewhere.⁷³ Because of the long-term nature of the parent study,⁷³ the glaucoma group were medicated, 10 exclusively with β -blockers and 7 also with miotics. The miotics led to a significant reduction in pupil diameter of approximately 27% compared with that in normal subjects ($P < 0.005$; Table 1).

The research followed the tenets of the Declaration of Helsinki. Informed written consent was obtained from the subjects after the nature and possible consequences of the study were explained to them. The research was approved by Australian National University's Human Experimentation Ethics Committee under protocol M 881.

Discriminant Analysis

The objective of this analysis was to determine whether the structure of the data permitted a method that was able to discriminate normal subjects from those with glaucoma. Note that the differing covariance of each group suggested the use of quadratic discriminant analysis (QDA).⁸⁴ Linear discriminant analysis (LDA)⁸⁴ was also conducted for comparison. The Appendix illustrates the two methods. Although the LDA models are simpler, LDA was less appropriate than QDA, given the different covariance structures of the data of normal subjects and those with glaucoma.⁸⁴ Sensitivities and specificities were estimated from receiver operator curves (ROCs), for which in LDA the risk factors were based on Fisher's linear discriminant function (equation A1), and the QDA classifier was the likelihood ratio assuming separate variance matrices.⁸⁴ Extensive details of LDA, QDA, and the use of ROCs have been given previously.⁷³

RESULTS

General Results

It was first necessary to determine whether significant zone amplitudes could be measured. We found that by averaging data from 4 to 12 trials of 40 seconds we could obtain four or more significant MFP zone amplitudes. The interaction frequencies ($f_i + f_j$) that would indicate interactions, or light scattering, between the nine stimulus zones were only occasionally significant, consistent with the 95% significance test (Fig. 2 and the Methods section). The average amplitudes for the different subject groups, normal subjects, and the weakly suspect, strongly suspect, and glaucoma groups, are shown in Figure 3. Notice that there were distinct regional differences and that these were maintained across the diagnostic groups. We also examined regional response amplitudes in a subgroup of eight normal subjects using visual stimuli in which the spatial frequencies were scaled up or down by four times compared with the normal case (Fig. 4). The finer stimuli proved the least reliable, with the coarser stimuli showing a regional amplitude variation similar to that obtained for the normal test stimuli (cf. Figs. 4A and 4B).

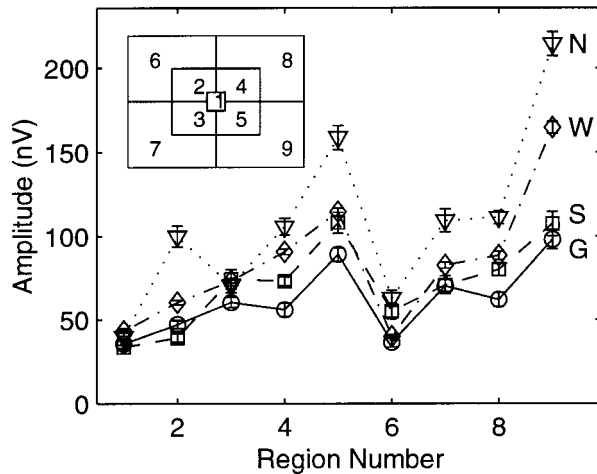


FIGURE 3. Average regional MFP response amplitudes by diagnostic group: N, normal; W, weakly suspect; S, strongly suspect; G, known glaucoma. Error bars are group SE. (*Inset*) The diagrammatic representation of the stimulus indicates the numbering scheme of the stimulus regions (zones). All eyes tested were right eyes, and visual field positions and retinal positions therefore corresponded in the same way for all subjects.

Discriminant Analysis

We next examined the sensitivity and specificity of the MFP. We took two basic approaches to this analysis. The first involved constructing discriminant models on so-called sorted measures, in which measures obtained from each stimulus region were sorted according to their reliability, thus biasing the analysis toward the most significant differences from normal performance. For the sorted data we examined the effect of the number of regional signals included in the analysis. The second approach involved making direct region-to-region comparisons.

Absolute phase was of little use. This was not unexpected, because at these frequencies small delays translate into phase shifts exceeding 1 cycle. Instead, we examined relative phase. We used the phase of region 9 as the reference phase for each data set, because it provided the most reliable signal (Figs. 2A, 3, 4B), being significant at $P < 0.001$ in 76% of all subjects and in all normal subjects at $P < 0.05$ or better. To construct the relative phase, we subtracted the phase of region 9 for a given subject from each of the nine regional phases. In this way, the phase of region 9 for all subjects was brought to 0° , and the phase lags and leads of the other regional responses relative to that of region 9 were preserved.

For both the sorted and rotated data sets, we examined amplitude and relative phase and amplitude relative to the geometric means across normal subjects. Both decibel and linear amplitude measures were considered. In a further analysis, we subtracted the (geometric) mean model for normal subjects from the amplitude data, and in other cases we divided by the mean model (equivalent to subtracting the decibel version from data transformed to decibels). This weighting operation was a conservative operation, because it scaled large, reliable signals downward and small, less reliable, MFP signals upward. For all the cases we examined linear (LDA) and quadratic (QDA) discriminant analysis models (see the Methods section and Appendix) in which the models were con-

structed from the data from our normal and glaucoma groups. These discriminant functions were then used to classify the subjects in the weakly and strongly suspect groups. Further details are supplied later for specific cases.

One of the simplest measures, regional amplitudes divided by the geometric mean for normal subjects, so-called scaled amplitudes, was the most reliable diagnostically, providing a sensitivity of 92.9% at 91.7% specificity for the linear discriminant model, and sensitivities and specificities of 100% for the quadratic case. Note that means and covariances for the normal and glaucoma groups were used to form the discriminant functions (equations A1 and A2) and then the vectors, \mathbf{x}_s , of nine scaled amplitudes from each subject were used as the inputs for classification (\mathbf{x}_0 in equations A1 and A2). Sorted amplitude differences from normal performance gave poor performance at 71.4% sensitivity for 75% specificity (simultaneously highest values, 85.7% specificity at 83.3% sensitivity for the quadratic case). Relative phase alone was as good as sorted amplitudes at 71.4% sensitivity for 75% specificity for LDA. There was no general pattern of relative phase changes with respect to visual field location. Including both amplitude and relative phase gave 100% sensitivity and specificity even in the LDA case. This was true for both scaled and unscaled amplitudes. In these models the vectors, \mathbf{x}_s , of nine amplitudes and nine relative phases from each subject were used as the

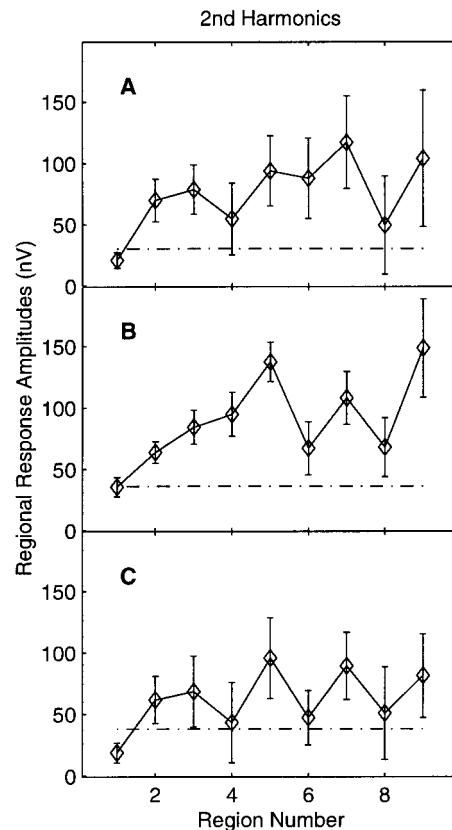


FIGURE 4. Average regional MFP response amplitudes for eight normal subjects for test stimuli having the spatial frequencies of each of their regions scaled: (A) Four times lower than the normal case, (B) the same as for the normal stimuli (Fig. 3), and (C) four times higher than normal. Error bars are group SE. The horizontal *dash-dot line* segment in each figure is the mean 95% confidence limit above which the signals are determined to be significant.

inputs for classification (\mathbf{x}_0 in equations A1 and A2). The scaled amplitude LDA model diagnosed 52.7% of weakly suspect eyes and 66.7% of strongly suspect eyes as glaucomatous. Performance for the QDA model was 50.0% and 60.0% for weakly and strongly suspect eyes, respectively.

DISCUSSION

The high sensitivities and specificities (100%) reported for the more complex quadratic discriminant models require further verification; however, even the simpler linear discriminant model using amplitude and relative phase performed at 100%. Of our 14 subjects with glaucoma 12 did not meet the strict HFA criteria of Caprioli⁸³ for glaucoma diagnosis although all met the moderate criteria. Thus, it could be argued that we were only matching HFA performance. Nevertheless, 67% of eyes that were strongly suspect had glaucoma diagnosed by the same analysis (see also Reference 82). Combined measures considering both the N95 and P50 component of the conventional PERG seem to provide sensitivity and specificity in the region of 95%¹³ for confirmed glaucoma. Relative phase appeared to add some extra information for discrimination of our data. Similarly, small effects have been reported for absolute phase in conventional PERGs.^{85,86}

Inspection of Table 1 shows that the mean defect (MD) and pattern standard deviations (PSDs) of our normal subjects were slightly high. Although this may at first seem at odds with our high reported sensitivities and specificities for the MFP method, it may also be related to earlier findings that HFA MD is not well correlated with glaucomatous damage.⁷³ In any case, improved diagnosis in our normal subjects would only improve our sensitivities and specificities.

The large MFP regions used in this study mean the detected loss was relatively diffusely distributed. This apparent diffuse loss is in accord with a study in which 330 subjects performed an FD-based contrast threshold test up to seven times over 2 years.⁷³ In that study the thresholds were obtained with large (FD) patterns similar to the MFP stimuli used in the this study, and the tests provided median sensitivities of 90.8% at specificities of 94%. These two studies indicate that tests based on the FD illusion can pick up diffuse early glaucomatous loss, as in the strongly suspect group in this study.⁸² Such a result is consistent with anatomical^{22-25,87} and conventional PERG studies,^{12,13,26} indicating diffuse cell loss in glaucoma.

An interesting feature of the MFP data was the differing responses by the different visual field quadrants over a 16-fold range of spatial frequencies (Fig. 4). Visual field dependencies similar to those found for our usual stimulus condition (Figs. 3, 4B) have been reported before in which the four quadrants were tested sequentially with an 8.33-Hz, 0.5-cyc/deg pattern.⁸⁸ A study examining the density of the units subserving the FD illusion has shown similar differences⁵³ that were found to be related to known anatomic retinal ganglion cell densities. Thus, it seems with these spatially coarse fast stimuli, we may be accessing a different retinal pathway. A study comparing the diagnostic utility for glaucoma of a range of low spatial frequencies, modulated at 27 Hz and presented in the periphery, showed that the usual spatial frequencies used in this study are approximately optimal for glaucoma diagnosis.⁸¹

Virtues of Using the M_y Pathway for the Early Detection of Retinal Damage

Examining the M_y -cell system may provide greater sensitivity to glaucomatous damage than examining other more populous systems.^{52,53} Improved sensitivity to damage would arise from two sources: cell size and retinal coverage factor. Early suggestions that in humans larger retinal ganglion cells were more susceptible to glaucomatous damage^{22,32-34} have been supported by many studies³¹⁻³⁴ indicating that primate retinal ganglion cell loss in glaucoma is proportional to ganglion cell size. The size dependence extends even to the fovea.²⁵ At least three studies indicate that M_y cells are larger than M_x cells.^{39,40,42}

As mentioned, perhaps the primary reason for M_y -cell sensitivity to glaucomatous damage may reside in retinal coverage factors.⁵¹⁻⁵³ Anatomical^{89,90} and electrophysiological⁴⁴ estimates of the ganglion cell coverage factors (or number of receptive fields/image point) range between 2 and 7 for M cells (cf. 24 for P cells⁴⁴; for review see Reference 91). Evidence from studies on humans⁵³ and macaques³⁹⁻⁴² indicates that the M_y cells make up 20% or less of the M pathway, and as a result their coverage factor could be less than 1. It follows that the performance of the M_y system would be particularly susceptible to any diffuse cell loss across the retina, because there would be little redundancy to hide the loss. Such low coverage factors would lead to spatial aliasing effects, which have been reported.^{51,53}

Problems

Perhaps the major problem with the present method is that in a few eyes we could not obtain significant amplitudes from all nine regions, even after 12 repeats. Some nonsignificant amplitudes can be expected in glaucoma; however, at 40 seconds per repeat this would make the method uncompetitive with frequency doubling technology (FDT; Zeiss Humphrey Systems, Dublin, CA) perimetry.^{71,72,74} ERG recording itself has its problems¹⁹ and advances in VEP recording methods for glaucoma³⁰ may make that avenue more attractive.

SUMMARY

PERG amplitudes measured for gratings scaled over a 16-fold range showed quite different visual field dependencies. These differences could reflect different retinal mechanisms being accessed by the differently scaled stimuli. PERG signal components associated with the FD illusion^{57,58,62} appear to be highly selective for glaucomatous damage. The good sensitivity obtained for our strongly suspect group (and not for the weakly suspect group) indicates that information about early glaucoma is obtained. The low spatial frequencies required to produce the FD illusion are a positive advantage from the clinical standpoint, because little demodulation of contrast can be expected even by ± 5 D of defocus.

Acknowledgments

The authors thank the reviewers for advisory assistance.

References

- Holländer H, Bisti S, Maffei L, Hebel R. Electroretinogram responses and retrograde changes of retinal morphology after intra-

- cranial optic nerve section A quantitative analysis in the cat. *Exp Brain Res*. 1984;55:483-493.
2. Maffei L, Fiorentini A. Electroretinographic responses to alternating gratings before and after section of the optic nerve. *Science*. 1981;211:953-954.
 3. Harrison JM, O'Connor PS, Young SL, Kincaid M, Bentley R. The pattern ERG in man following surgical resection of the optic nerve. *Invest Ophthalmol Vis Sci*. 1987;28:492-499.
 4. Sieving PA, Steinberg RH. Proximal retinal contribution to the intraretinal 8-Hz pattern ERG of cat. *J Neurophysiol*. 1987;57:104-120.
 5. Baker CL, Hess RR, Olsen BT, Zrenner E. Current source density analysis of linear and nonlinear components of the primate electroretinogram. *J Physiol*. 1988;407:155-176.
 6. Shapley RM, Perry VH. Cat and monkey retinal ganglion cells and their visual functional roles. *Trends Neurosci*. 1986;9:229-235.
 7. Kolb H, Nelson R, Mariani A. Amacrine cells, bipolar cells and ganglion cells of the cat retina: a Golgi study. *Vision Res*. 1981;21:1081-1114.
 8. Kolb H, Linberg KA, Fisher SK. Neurons of the human retina. *J Comp Neurol*. 1992;318:147-187.
 9. Mariani AP. Amacrine cells of the monkey retina. *J Comp Neurol*. 1990;301:382-400.
 10. Vaney DI. The mosaic of amacrine cells in the mammalian retina. *Prog Retinal Res*. 1990;9:49-100.
 11. Zrenner E. The physiological basis of the pattern electroretinogram. *Prog Retinal Res*. 1990;9:427-464.
 12. Falsini B, Colotto A, Porciatti V, Porrelo G. Follow-up study with pattern ERG in ocular hypertension and glaucoma patients under timolol maleate treatment. *Clin Vision Sci*. 1992;7:341-347.
 13. O'Donoghue E, Arden GB, O'Sullivan F, et al. The pattern electroretinogram and ocular hypertension. *Br J Ophthalmol*. 1992;76:387-394.
 14. Pfeiffer N, Tillmon B, Bach M. Predictive value of the pattern electroretinogram in high-risk ocular hypertension. *Invest Ophthalmol Vis Sci*. 1993;34:1710-1715.
 15. Trick GL. Retinal potentials in patients with primary open-angle glaucoma: physiological evidence for temporal frequency tuning effects. *Invest Ophthalmol Vis Sci*. 1985;26:1750-1758.
 16. Towle VL, Moskowitz A, Sokol S, Schwartz B. The visual evoked potential in glaucoma and ocular hypertension: effects of check size, field size, and stimulation rate. *Invest Ophthalmol Vis Sci*. 1983;24:175-183.
 17. Marx MS, Podos SM, Bodis-Wollner I, Lee PY, Wang RF, Severin C. Signs of early damage in glaucomatous monkey eyes, low spatial frequency losses in the pattern ERG and VEP. *Exp Eye Res*. 1988;46:173-184.
 18. Johnson MA, Drum BA, Quigley HA, Sanchez RM, Dunkelberger GR. Pattern-evoked potentials and optic nerve fiber loss in monocular laser-induced glaucoma. *Invest Ophthalmol Vis Sci*. 1989;30:897-907.
 19. Graham SL, Klistorner A. Electrophysiology: a review of signal origins and applications to investigating glaucoma. *Aust N Z J Ophthalmol*. 1998;26:71-85.
 20. Wässle H, Grünert U, Röhrenbeck J, Boycott BB. Cortical magnification factor and the retinal ganglion cell density of the primate retina. *Nature*. 1989;30:643-646.
 21. Wässle H, Grünert U, Röhrenbeck J, Boycott BB. Retinal ganglion cell density and cortical magnification factor in the primate. *Vision Res*. 1990;30:1897-1911.
 22. Quigley HA, Addicks EM, Green RW. Optic nerve damage in human glaucoma, III: quantitative correlation of nerve fibre loss and visual field defect in glaucoma, ischaemic neuropathy, papilloedema and toxic neuropathy. *Arch Ophthalmol*. 1982;100:135-146.
 23. Airaksinen PJ, Lukowski R, Drance SM, Price M. Colour vision and retinal nerve fiber layer in early glaucoma. *Am J Ophthalmol*. 1986;101:208-213.
 24. Schulzer M, Mikelberg FS, Drance SM. A study of the value of the central and peripheral isoptres in assessing visual field progression in the presence of paracentral scotoma measurements. *Br J Ophthalmol*. 1987;71:422-427.
 25. Glovinsky Y, Quigley HA, Pease ME. Foveal ganglion cell loss is size dependent in experimental glaucoma. *Invest Ophthalmol Vis Sci*. 1993;34:395-400.
 26. Bach M, Pfeiffer N, Birkner-Binder D. Pattern electroretinogram reflects diffuse retinal damage in early glaucoma. *Clin Vis Sci*. 1992;7:335-340.
 27. Caprioli J. Automated perimetry in glaucoma. *Am J Ophthalmol*. 1991;111:235-239.
 28. Zrenner E, Nelson R. Spatial characteristics of scotopic threshold responses in the corneally recorded electroretinogram elicited by multispot patterns. *Clin Vision Sci*. 1988;3:29-44.
 29. Pfeiffer N, Birkner-Binder D, Bach M. Das Muster-ERG bei okulärer Hypertension und Glaukom: Einfluss von Karogröße, Kontrast und retinaler Exzentrizität. *Fortschr Ophthalmol*. 1991;88:815-818.
 30. Klistorner A, Graham S, Grigg J, Billson F. Multifocal topographic visual evoked potential: improving objective detection of local visual field defects. *Invest Ophthalmol Vis Sci*. 1998;39:937-950.
 31. Glovinsky Y, Quigley HA, Dunkelberger GR. Retinal ganglion cell loss is size dependent in experimental glaucoma. *Invest Ophthalmol Vis Sci*. 1991;32:484-491.
 32. Quigley H, Sanchez R, Dunkelberger GR, L'Hernault NL, Baginski TA. Chronic glaucoma selectively damages large optic nerve fibres. *Invest Ophthalmol Vis Sci*. 1987;28:913-920.
 33. Quigley HA, Dunkelberger GR, Green WR. Chronic human glaucoma causing selectively greater loss of large optic nerve fibres. *Ophthalmology*. 1988;95:357-367.
 34. Quigley HA, Dunkelberger GR, Green WR. Studies of retinal ganglion cell atrophy correlated with automated perimetry in human eyes with glaucoma. *Am J Ophthalmol*. 1989;107:453-464.
 35. Quigley H, Kerrigan-Baumrind L, Pease M, Kerrigan D, Mitchell R. The number of retinal ganglion cells in glaucoma eyes compared with threshold visual field data in the same eyes [ARVO Abstract]. *Invest Ophthalmol Vis Sci*. 1999;40(4):S582. Abstract nr 3059.
 36. Polyak SL. *The Retina*. Chicago: University of Chicago Press; 1941.
 37. Grünert U, Greferath U, Boycott BB, Wässle H. Parasol (Pa) ganglion-cells of the primate fovea: immunocytochemical staining with antibodies against GABA-a receptors. *Vision Res*. 1993;33:1-14.
 38. Enroth-Cugell C, Robson JG. The contrast sensitivity of retinal ganglion cells of the cat. *J Physiol*. 1966;187:517-522.
 39. Kaplan E, Shapley RM. X and y cells in the lateral geniculate nucleus of macaque monkeys. *J Physiol*. 1982;330:125-143.
 40. Marrocco RT, McClurkin JW, Young RA. Spatial summation and conduction latency classification of cells of the lateral geniculate nucleus of macaques. *J Neurosci*. 1982;2:1275-1291.
 41. Derrington AM, Lennie P. Spatial and temporal contrast sensitivities of neurones in lateral geniculate nucleus of macaque. *J Physiol*. 1984;357:219-240.
 42. Blakemore C, Vital-Duran F. Organization and post-natal development of the monkey's lateral geniculate nucleus. *J Physiol*. 1986;380:453-491.
 43. Kaplan E, Shapley RM. The primate retina contains two types of ganglion cells, with high and low contrast sensitivity. *Proc Natl Acad Sci USA*. 1986;83:2755-2757.
 44. Crook JM, Lange-Maleki B, Lee BB, Valberg A. Visual resolution of macaque retinal ganglion cells. *J Physiol*. 1988;396:205-224.
 45. Michael CR. Retinal afferent arborization patterns, dendritic field orientations, and the segregation of function in the lateral geniculate nucleus of the monkey. *Proc Natl Acad Sci USA*. 1988;85:4914-4917.
 46. Purpura K, Kaplan E, Shapley RM. Background light and the contrast gain of primate P and M retinal ganglion cells. *Proc Natl Acad Sci USA*. 1988;85:4534-4537.
 47. Purpura K, Trachina D, Kaplan E, Shapley RM. Light adaptation in the primate retina: analysis of changes in the gain and dynamics of monkey retinal ganglion cells. *Vis Neurosci*. 1990;4:75-93.
 48. Dacey DM, Brace S. A coupled network for parasol but not midget ganglion cells in the primate retina. *Vis Neurosci*. 1992;9:279-290.
 49. Vaney DI. Many diverse types of retinal neurons show tracer coupling when injected with biocytin or neurobiotin (letter). *Neurosci*. 1991;125:187-190.

50. Blakemore C, Vital-Durand F. Distribution of x- and y-cells in the monkey's lateral geniculate nucleus. *J Physiol.* 1981;320:17P.
51. Maddess T, Henry GH. Density of nonlinear visual units and glaucoma [ARVO Abstract]. *Invest Ophthalmol Vis Sci.* 1990;31(4):S231. Abstract nr 1134.
52. Maddess T, Henry GH. Nonlinear visual responses and visual deficits in ocular hypertensive and glaucoma subjects. *Clin Vis Sci.* 1992;7:371-383.
53. Maddess T, James AC, Hemmi J. Evidence for spatial aliasing effects in the Y-like cells of the magnocellular visual pathway. *Vision Res.* 1998;38:1843-1859.
54. Kelly DH. Nonlinear visual responses to flickering sinusoidal gratings. *J Opt Soc Am.* 1981;71:1051-1055.
55. Kelly DH. Frequency doubling in visual responses. *J Opt Soc Am.* 1966;56:1628-1633.
56. Tyler CW. Observations on spatial-frequency doubling. *Perception.* 1974;3:81-86.
57. Maddess T, Bedford S, James AC, Rose KA. A multiple frequency, multiple region pattern electroretinogram investigation of nonlinear retinal signals. *Aust N Z J Ophthalmol.* 1997;25:94-97.
58. Bedford S, Maddess T, Rose KA, James AC. Correlations between observability of the spatial frequency doubled illusion, a multi-region PERG. *Aust N Z J Ophthalmol.* 1997;25:91-93.
59. Maddess T, Kulikowski JJ. Apparent finess of stationary compound gratings. *Vision Res.* 1999;39:3404-3416.
60. Kulikowski JJ. Apparent fineness of briefly presented gratings: balance between movement and pattern channels. *Vision Res.* 1975;15:673-680.
61. Victor JD. The dynamics of the cat retinal Y cell subunit. *J Physiol.* 1988;405:289-320.
62. James AC, Maddess T, Rouhan K, Bedford S, Snowball M. Evidence for My-cell involvement in the spatial frequency doubled illusion as revealed by a multiple region PERG for Glaucoma. *J Opt Soc Am.* 1995;1:314-317.
63. Shapley RM, Victor JD. The effect of contrast on the non-linear response of the Y-cell. *J Physiol.* 1980;302:535-547.
64. Victor JD, Shapley RM. The nonlinear pathway of Y ganglion cells in the cat retina. *J Gen Physiol.* 1979;74:671-689.
65. Shapley RM, Victor JD. How the contrast gain control modifies the frequency responses of cat retinal ganglion cells. *J Physiol.* 1981;318:161-179.
66. Benardete EA, Kaplan E, Knight BW. Contrast gain control in the primate retina: P cells are not X-like, some M cells are. *Vis Neurosci.* 1992;8:483-486.
67. Benardete EA, Kaplan E. The dynamics of primate retinal ganglion cells. *Vis Neurosci.* 1999;16:344-368.
68. Victor JD. The dynamics of the cat retinal X cell centre. *J Physiol.* 1987;386:219-246.
69. Victor JD, Shapley RM. Receptive field mechanisms of cat X and Y retinal ganglion cells. *J Gen Physiol.* 1979;74:257-298.
70. James AC, Maddess T. Glaucoma testing using non-linear systems identification techniques, 1996; US Patent No. 5,539,482.
71. Maddess T. Method and apparatus for use in diagnosis of glaucoma. US patent 5,065,767; 1991.
72. Maddess TL. Early detection of glaucoma. US Patent 5,912,723; 1995.
73. Maddess T, Goldberg I, Dobinson J, Wine S, Welch AH, James A. Testing for glaucoma with the frequency doubled illusion. *Vision Res.* 1999;39:4258-4273.
74. Johnson CA, Samuels S. Screening for glaucomatous visual field loss with frequency doubling perimetry. *Invest Ophthalmol Vis Sci.* 1997;38:413-425.
75. Sponsel W, Argano S, Trigo Y, Mensah J. Clinical classification of glaucomatous visual field loss by frequency doubling perimetry. *Am J Ophthalmol.* 1998;125:830-836.
76. Quigley H. Identification of glaucoma-related visual field abnormality with the screening protocol of frequency doubling technology. *Am J Ophthalmol.* 1998;125:819-829.
77. Blumenthal EZ, Sample PA, Zangwill L, Lee AC, Kono Y, Weinreb RN. Comparison of long-term variability for standard and short-wavelength automated perimetry in stable glaucoma patients. *Am J Ophthalmol.* 2000;129:309-313.
78. Burnstein Y, Elish NJ, Magbalon M, Higginbottom EJ. Comparison of frequency doubling perimetry with Humphrey visual field analysis in a glaucoma practice. *Am J Ophthalmol.* 2000;129:328-333.
79. Cello KE, Nelson-Quigg JM, Johnson CA. Frequency doubling perimetry for detection of glaucomatous field loss. *Am J Ophthalmol.* 2000;129:314-322.
80. Patel SC, Friedmann DS, Varadkar P, Robin AL. Algorithm for interpreting the results of frequency doubling perimetry. *Am J Ophthalmol.* 2000;129:323-327.
81. Maddess T, Severt WL. Testing for glaucoma with the frequency doubling illusion in the whole, macular and eccentric visual fields. *Aust N Z J Ophthalmol.* 1999;27:194-196.
82. Maddess T, James AC, Goldberg I, Wine S, Dobinson J. Comparing a parallel PERG, automated perimetry, and frequency-doubling thresholds. *Invest Ophthalmol Vis Sci.* 2000;41:3827-3832.
83. Caprioli J. Automated perimetry in glaucoma. In: Walsh TJ, ed. *Visual Fields Examination and Interpretation.* San Francisco: American Academy of Ophthalmology; 1990:71-106.
84. Johnson RA, Wichern DW. *Applied Multivariate Statistical Analysis.* 3rd ed. Englewood Cliffs, NJ: Prentice-Hall; 1992.
85. Korth M, Horn F, Storck B, Jost J. The pattern-evoked electroretinogram (PERG): age related alterations and changes in glaucoma. *Graefes Arch Clin Exp Ophthalmol.* 1989;27:123-130.
86. Falsini B, Colotto A, Porciatti V, Buzzontelli L, Coppe A, De Luca LA. Macular flicker- and pattern-ERGs are differently affected in ocular hypertension and glaucoma. *Clin Vision Sci.* 1991;6:423-429.
87. Harwerth RS, Carter-Dawson L, Shen F, Smith EL III, Crawford MJL. Ganglion cell losses underlying visual field defects from experimental glaucoma. *Invest Ophthalmol Vis Sci.* 1999;40:2242-2250.
88. Horn F, Mardin C, Korth M, Martus P. Quadrant pattern ERG with SLO stimulation in normals and glaucoma patients. *Graefes Arch Clin Exp Ophthalmol.* 1996;234(suppl 1):S174-S179.
89. Perry VH, Cowey A. The ganglion cell and cone distributions in the monkey's retina: implications for central magnification factors. *Vision Res.* 1985;25:1795-1810.
90. Grünert U, Martin PR. Rod bipolar cells in the macaque monkey retina: immunoreactivity and connectivity. *J Neurosci.* 1991;11:2742-2758.
91. Lee BB. Receptive field structure in the primate retina. *Vision Res.* 1996;36:631-644.

APPENDIX

Suppose there are m observations of the multivariate random variable $X' = (X_1, X_2 \dots X_p)$ from population π_1 , and n observations of the same format from population π_2 . From these data sets the correct classification is assumed to be known. The technique of discriminant analysis derives a classification rule for any new data point, which seeks to minimize the cost of a misclassification.

Let us assume that:

1. The two populations have probability density functions $f_1(x)$ and $f_2(x)$ respectively.
2. The probabilities of a new data point coming from populations π_1 or π_2 is p_1 and $p_2 = 1 - p_1$ respectively (the prior probabilities).
3. The cost of misclassifying a point that is really from population π_1 as being from the other population is C_1 , and the cost of misclassifying a point that is really from population π_2 as being from the other population is C_2 .

Note that the probability density function $f_1(x)$ is the conditional probability density for observing the value x , given that the point came from population π_1 . The joint probability density of observing the value x and that the point came from

π_1 is thus $f_1(x)p_1$, and the marginal probability of observing the value x irrespective of the class is $f(x) = f_1(x)p_1 + f_2(x)p_2$.

Bayes' rule can be used to invert the conditional probabilities: The probability that an observed value x came from population π_1 is $p(\pi_1|x) = f_1(x)p_1/f(x)$, and the probability that it came from population π_2 is $p(\pi_2|x) = f_2(x)p_2/f(x)$.

For a given new observation x , the expected cost if we assign to class 2 is the probability that it was really from population 1 multiplied by that cost: $C_1f_1(x)p_1/f(x)$. The expected cost if we assign to class 1 is likewise $C_2f_2(x)p_2/f(x)$.

The optimal rule is now clear: We should assign to class 1 if that expected cost is less—that is, if

$$C_2f_2(x)p_2/f(x) < C_1f_1(x)p_1/f(x)$$

Rearranging, this is true when

$$f_1(x)/f_2(x) > (C_2/C_1)(p_2/p_1)$$

or, taking the natural logarithms, a monotonic increasing function,

$$\log[f_1(x)/f_2(x)] > \log[(C_2/C_1)(p_2/p_1)]$$

The further assumption may be made that each of the two populations follows a multivariate normal distribution, for which we estimate the population mean vectors by the sample means \mathbf{u}_1 and \mathbf{u}_2 ($p \times 1$), and we estimate the population covariance matrices by the sample covariance matrices, \mathbf{S}_1 and \mathbf{S}_2 ($p \times p$).

If the covariances are assumed to be equal, they are both estimated by the pooled covariance, $S_{\text{pooled}} = [(m - 1)\mathbf{S}_1 + (n - 1)\mathbf{S}_2]/(m + n - 2)$. The multivariate normal probability density for population π_1 is then estimated as

$$f_1(x) = (2\pi)^{-p/2} \det(\mathbf{S})^{-1/2} \exp[-1/2(\mathbf{x} - \mathbf{u}_1)' \mathbf{S}^{-1}(\mathbf{x} - \mathbf{u}_1)]$$

and likewise for population π_2 . The condition for assigning to class 1 using the logarithm of the ratio is

$$[-1/2(\mathbf{x} - \mathbf{u}_1)' \mathbf{S}^{-1}(\mathbf{x} - \mathbf{u}_1)] - [-1/2(\mathbf{x} - \mathbf{u}_2)' \mathbf{S}^{-1}(\mathbf{x} - \mathbf{u}_2)] > \log[(C_2/C_1)(p_2/p_1)]$$

and can be rearranged as

$$(\mathbf{u}_1 - \mathbf{u}_2)' \mathbf{S}^{-1} \mathbf{x} + 1/2 \mathbf{u}_2' \mathbf{S}^{-1} \mathbf{u}_2 - 1/2 \mathbf{u}_1' \mathbf{S}^{-1} \mathbf{u}_1 > \log[(C_2/C_1)(p_2/p_1)]$$

This condition can be written in the form

$$\mathbf{b} \mathbf{x}_0 + c > 0 \tag{A1}$$

where c is a scalar and \mathbf{b} is a row vector of coefficients. This is sometimes referred to as Fischer's linear discriminant or classification rule.

If the covariance matrices are not equal, i.e., $\mathbf{S}_1 \neq \mathbf{S}_2$, then the resultant rule is to classify an observation \mathbf{x}_0 as being from population 1 (π_1) if the following quadratic condition holds.

$$\mathbf{x}_0' \mathbf{A} \mathbf{x}_0 + \mathbf{b}' \mathbf{x}_0 + c > 0 \tag{A2}$$

where

$$\mathbf{A} = 1/2(\mathbf{S}_2^{-1} - \mathbf{S}_1^{-1})$$

$$\mathbf{b} = -1/2(\mathbf{u}_2' \mathbf{S}_2^{-1} - \mathbf{u}_1' \mathbf{S}_1^{-1})$$

$$c = 1/2(\mathbf{u}_2' \mathbf{S}_2^{-1} \mathbf{u}_2 - \mathbf{u}_1' \mathbf{S}_1^{-1} \mathbf{u}_1) + 1/2 \log[\det(\mathbf{S}_2)/\det(\mathbf{S}_1)] - \log[(C_2/C_1)(p_2/p_1)]$$

Geometrically, the linear discriminant function defines a decision boundary, or separatrix, that is a (possibly diagonal) straight line across the plane in the case of a bivariate observation and in general is a hyperplane in the multivariate case. The quadratic discriminant rule defines a decision boundary that is (possibly rotated) a parabola in the bivariate case and is a paraboloidal surface in the general multivariate case (for examples see⁷³).